Detection of lead in bone phantoms and arsenic in soft tissue phantoms using synchrotron radiation and a portable x-ray fluorescence system

Craig Groskopf [1], Stephen R. Bennett [1], Mihai R. Gherase[2], and David E.B. Fleming[1].

[1] Physics Department, Mount Allison University, Sackville, NB, Canada
[2] Physics Department, California State University, Fresno, Fresno, CA, USA

Corresponding Author e-mail: dfleming@mta.ca; phone: (506) 364-2584

Abstract

The differences and commonalities between x-ray fluorescence results obtained using synchrotron radiation and a portable x-ray fluorescence device were examined using arsenic in soft tissue phantoms and lead in bone phantoms. A monochromatic beam energy of 15.8 keV was used with the synchrotron, while the portable device employed a rhodium anode x-ray tube operated at 40 kV. Bone phantoms, dosed with varying quantities of lead, were made of Plaster of Paris and placed underneath skin phantoms of either 3.1 mm or 3.9 mm thickness. These skin phantoms were constructed from polyester resin, and dosed with varying amounts of arsenic. Using an irradiation time of 120 seconds, arsenic Kα and Kβ, and lead Lα and Lβ characteristic x-ray peaks were analysed. This information was used to calculate calibration line slopes and minimum detection limits for each data set. As expected, minimum detection limits were much lower at the synchrotron for detecting arsenic and lead. Both approaches produced lower detection limits for arsenic in soft tissue than for lead in bone when simultaneous detection was attempted. Although arsenic Kα and lead Lα emissions share similar energies, it was possible to detect both elements in isolation by using the arsenic Kβ and lead Lβ characteristic x-rays. Greater thickness of soft tissue phantom reduced the ability to detect the underlying lead. Experiments with synchrotron radiation could help guide future efforts toward optimizing a portable x-ray fluorescence *in vivo* measurement device.

Keywords: lead, arsenic, synchrotron, portable XRF

Introduction

Chronic exposure to lead from occupational hazards or the general environment is known to be toxic to humans, predominantly affecting the central nervous system. To measure recent exposure to lead, blood lead is commonly used, however bone is where the majority of the body burden lies [Goyer 1993]. The half-life of lead in bone spans from several years to decades [Rabinowitz 1991]. This makes bone lead ideal for evaluating long term lead exposure.

Like lead, long term exposure to arsenic is linked to negative health effects. Exposure to arsenic is often from drinking water, and can result in an increased risk to develop diabetes, cardiovascular disease, and cancer [Abernathy *et al*. 2003]. Arsenic has a tendency to bind with keratin, making skin a key site for arsenic accumulation [Schwartz 1997]. An interesting property of lead and arsenic is that the characteristic x-ray Lα emission line of lead and the characteristic x-ray Kα emission line of arsenic are both ~10.5 keV in energy. This can create problems when attempting to detect both elements simultaneously, as the two peaks sum into one larger peak.

Applications for portable x-ray fluorescence in human trace element detection have been explored, initially using phantoms to simulate the human body. Recent phantom-based work has included feasibility studies of the detection of lead in bone [Nie *et al*. 2011; Fleming *et al*. 2011], manganese and zinc in nail clippings [Fleming *et al*. 2013], and arsenic in skin [Fleming and Gherase 2007]. There have also been studies which have measured bone lead *in vivo* using both portable L-shell [Specht *et al*. 2016] and (more commonly) larger K-shell x-ray fluorescence systems [Somervaille *et al*. 1985; Fleming *et al*. 1997]. Using a portable x-ray fluorescence

system offers many advantages. Such systems are relatively inexpensive, simple to use, provide results quickly, and can be brought to remote areas of the globe with ease.

Synchrotron radiation can also be used for x-ray fluorescence analysis. Although more difficult to access than portable x-ray fluorescence systems, synchrotrons offer other advantages. These facilities generally have reduced background interference, and a much smaller x-ray beam size. They are also significantly more powerful than a portable x-ray device, and the incident energy of the x-ray beam can be changed by the user [Grolimunda *et al*. 2004].

The use of x-ray fluorescence for the detection of lead and arsenic in humans has been studied in the past. For example, one paper argued that the amount of arsenic normally expected within soft tissue in the human body is not high enough to greatly interfere with the detection of lead in bone [Todd 2002]. Another study reported that bone lead L-shell x-ray fluorescence is prone to unacceptably high uncertainty due to factors such as radiation attenuation from overlying soft tissue [Todd *et al.* 2002]. However, with recent improvements in portable x-ray fluorescence technology and the reporting of *in vivo* L-shell bone lead measurements, it was considered worthwhile to revisit the issue of simultaneous assessment of arsenic and lead.

In the current paper, x-ray fluorescence results obtained from a synchrotron facility are compared to those from a new portable x-ray fluorescence system, highlighting the differences and commonalities between the two approaches. By isolating certain features of the measurements, it is expected that methods employing portable XRF can be improved upon for the future. The paper also considers the simultaneous detection of lead in bone and arsenic in soft tissue, and the associated challenges.

Methods

To model bone found in the human body, phantoms were created using Plaster of Paris (calcium sulphate hemihydrate; $CaSO_4$ ½ (H_2O)) which had been dosed with varying quantities of lead solution to create a range of concentrations. These phantoms had been available from previous work, and were in concentrations of 0, 7, 17, 26, and 34 μg Pb g^{-1} [Fleming *et al*. 2011]. Uncertainties in the individual concentrations were estimated to be 1 μg Pb g^{-1}. To create these phantoms, plaster was mixed with distilled water, and for each phantom containing lead, an appropriate volume of lead atomic absorption spectrometry standard solution (Sigma-Aldrich; Oakville, ON) was added using an adjustable volume pipettor. After vigorous stirring, the mixture was poured into plastic molds and allowed to set. To remove the phantoms from the plastic molds, gentle heating from a heat gun was used. The final samples had a square cross section of 2.2 cm × 2.2 cm.

Soft tissue phantoms were created using fiberglass resin (Bondo Corp. Atlanta, GA) following a previously used method [Fleming and Gherase 2007]. The resin was poured into a beaker and weighed, followed by the addition of an arsenic atomic absorption spectrometry standard solution (Sigma-Aldrich; Oakville, ON) using an adjustable volume pipettor. After vigorous stirring, a resin hardening catalyst was added, and the resin was poured into circular molds and allowed to harden for several days. A total of 8 phantoms were created using two thicknesses (thin, 3.1 mm; and thick, 3.9 mm) and four concentrations (0, 2, 5 and 10 μg As g^{-1}). After hardening, the resin was cut into squares measuring approximately 2 cm on each side.

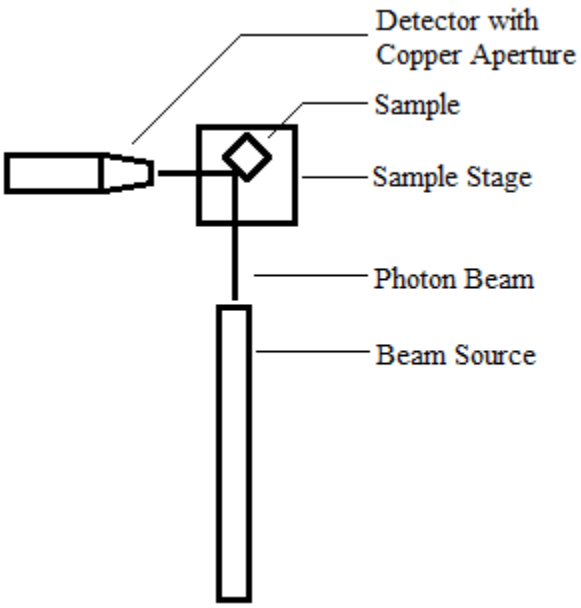

Figure 1. Simple diagram of experimental setup at the Canadian Light Source synchrotron.

The phantoms were then transported to the Canadian Light Source (CLS) to be analyzed using the VESPERS (Very sensitive Elemental and Structural Probe Employing Radiation from a Synchrotron) beamline. VESPERS is a hard x-ray beamline capable of producing energies between 6 and 30 keV [Desouza *et al*. 2013]. This particular beamline was selected due to its range of available beam energies, the possibilities for monochromatic excitation, and its beam size. The incident x-ray beam was polarized in the horizontal plane, parallel to the floor. This was also the plane defined by the beam, the sample, and the detector, thereby reducing the detected scatter component. The beam was aligned with the sample using a camera and an adjustable sample stage, with the beam creating a 45 degree angle with the sample. A Vortex ME4 4-element silicon drift detector (SII, Torrance, CA) was placed 1.5 cm away from the sample at a 45 degree angle (90 degrees from the incident beam) to record the fluorescence spectrum (See figure 1). A custom made tapered copper aperture with a 1.5 cm diameter was

placed over the detector to reduce contamination from stray x-rays. A split ion chamber with nitrogen gas was used to monitor the incident beam. A split ion chamber is formed from a pair of split anodes in an ionization chamber, where the two anode plates collect ions produced by the x-ray beam passing through an inert gas. The null difference between the two output currents indicates if the incident beam is centered on the ion chamber. Thus, the beam vertical position is monitored as well as the photon fluence rate of the incident beam (which is proportional to the sum of the two currents). The photon fluence rate was calculated to be ~1.6 x 10^{10} mm^{-2} s^{-1} at a storage ring current of ~185 mA. The beamline was configured to operate with incident energies of 15.8 keV, 16.6 keV and 17.5 keV with a 1.6% monochromatic bandpass and a beam size of 1 mm. In this paper, only an incident energy of 15.8 keV will be considered, as it efficiently excites both lead L-shell and arsenic K-shell electrons [Williams 2001], and was found to provide the best results. Results from all three energies will be explored in a future paper concerning lead measurement.

Beginning with the bone phantoms, each sample was placed on the stage and scanned for a total of 120 seconds. After scanning all bone phantoms, a soft tissue phantom was attached to the sample using a rubber band. To ensure the same orientation of the soft tissue phantom was used each time, a mark was added to the upper right corner using a permanent marker. This continued until all combinations of bone and soft tissue phantoms, including both soft tissue thicknesses, were scanned. Energy spectra (channel width of 0.01 keV) were recorded from each measurement, and analyzed as described below.

Following the trials at the synchrotron, the samples were scanned on a new portable x-ray fluorescence analyzer. The analyzer, an Olympus Innov-X Delta Premium (Innov-X Technologies Canada, Vancouver, BC) was operated in an integrated test stand provided by the

manufacturer. This system uses a silicon drift detector, with a rhodium anode x-ray tube operated at 40 kV and a beam current of 100 μA. The average photon energy (arithmetic mean) striking a sample is ~24 keV, and the x-ray beam has a diameter of ~9 mm at the location where samples are placed. A laptop computer (Dell Canada Inc, North York, ON) is used to operate the device and store the created spectra. Spectra from each bone phantom were collected from 5 separate trials, each lasting 120 seconds. The soft tissue phantoms were then placed on the analyzer, with the bone phantoms on top, for each possible combination of soft tissue and bone. Energy spectra were obtained from 5 separate 120 second trials for each combination. These spectra had a channel width of 0.02 keV.

The analysis of the spectra produced by the portable x-ray fluorescence analyzer was very similar to a previously described method [Gherase and Fleming 2011]. The number of counts recorded in each energy channel over the five trials was converted to a weighted average (N_{wa}) using the following formula:

$$N_{wa} = \frac{\sum_{i=1}^{5} w_i N_i}{\sum_{i=1}^{5} w_i}, \quad (1)$$

where N_i is the number of counts in each channel and w_i is the statistical weight. Due to time limitations at the CLS synchrotron, only one trial was performed for each sample, eliminating the need for a weighted average.

The average weighted spectra from the portable XRF system and the spectra from the CLS were fitted over the energy range of interest using a least-square nonlinear fitting routine in OriginPro 9.1 (OriginLab Co., Northampton, MA). The fitting routine consisted of a number of Gaussian peaks fitted over an exponential background, producing a function of the form:

$$f(x) = \sum_i^n G(x, a_i, b_i, c_i) + a_0 e^{b_0 x} + c_0 \quad (2)$$

$$G(x, a_i, b_i, c_i) = a_i e^{-b_i(x-c_i)^2} \quad (3)$$

In the above, f is a function of the energy (x), having a Gaussian peak G(x) with amplitude a_i, inverse width parameter b_i, and centered at c_i added for each peak in the spectrum. The background portion of the function was a simple exponential, with amplitude a_0, width b_0 and intercept c_0. Each spectrum had 4 or 5 peaks to fit, and included peaks for the Kα and Lα lines of lead and arsenic at 10.5 keV, the Kβ of arsenic at 11.7 keV and the Lβ of lead at 12.6 keV. Other peaks that were modeled include bromine at 11.9 keV, and gold at 11.4 keV. Bromine and gold are trace contaminants found in the commercial resin and the portable XRF system, respectively. In order to account for varying beam intensity at the CLS, the peak amplitudes from the synchrotron were normalized, by dividing the amplitudes by the average of the two voltages recorded by the split ion chamber. The amplitudes found in the analysis were then plotted against the known concentration of lead in each sample, while maintaining a constant arsenic concentration, and the known concentration of arsenic while maintaining a constant concentration of lead. These second plots were fitted with a standard linear fit routine provided in the OriginPro program, and were used to create a calibration line. The slope of this calibration line was then used to calculate the minimum detection limit using the following equation:

$$MDL = \frac{3\sigma_0}{a} \quad (4)$$

In this equation, σ_0 is the uncertainty of the peak amplitude with either no lead or no arsenic, and a represents the slope of the calibration line. The factor of 3 is used to provide a more rigorous detection limit.

During the analysis, it was found that some of the detected CLS peak amplitudes were much too low to be considered valid, given the experimental configuration. Although the cause of this

effect was not certain, it was most likely due to an error in the placement of the sample, preventing characteristic x-rays from reaching the detector properly and severely reducing counts. This effect was most common when the 34 ppm lead bone phantom was used. Because of this, all data points with the 34 ppm bone lead concentration taken at the CLS were removed from the analysis. The data points associated with 26 ppm of lead in bone with 5 ppm of arsenic in thin soft tissue and 26 ppm of lead in bone with 2 ppm of arsenic in thin soft tissue collected at the CLS were also removed for similar reasons. No similar effects were observed from the portable XRF system.

Results

Figure 2 shows typical x-ray spectra for the area of interest when detecting lead and arsenic. These spectra all have a thin 5 ppm arsenic soft tissue phantom overlaying a bone phantom dosed with lead. The largest peak in all four spectra at 10.5 keV is a combination of lead Lα and arsenic Kα. The arsenic Kβ peak, which is found at 11.7 keV, is broadened by interference from bromine, which is found at 11.9 keV. Spectra collected from the InnovX portable XRF system (Figure 2 c) and d)) had the additional contaminant of gold's Lβ line, which is seen at 11.4 keV. Finally, the lead Lβ peak is seen at 12.6 keV on all four spectra. The four spectra shown have all been fit using the function described in the methods.

Figure 3 displays the calibration slope graphs created by plotting the peak amplitude (of either the lead Lα or arsenic Kα emission line) against concentration. The lower line with the more shallow slope was created from the InnovX portable XRF system. The line with the larger slope was created from data collected from the CLS synchrotron. Figure 3 a) was created using peak amplitudes from the lead Lα peak at 10.5 keV, while using a 0 ppm arsenic thin soft tissue phantom. Figure 3 b) was created using peak amplitudes from the arsenic Kα peak, while using 0

μg Pb g^{-1} in a bone phantom and varying the arsenic concentration in thin soft tissue phantoms. Note that figure 3 a) also includes the 34 ppm lead data point which, as described in the methods, was removed from the linear fit analysis.

Tables 1 through 4 show the calibration slopes and intercepts created from varying lead or arsenic concentrations, when using either no soft tissue samples ("bare phantom"), thin soft tissue samples, or thick soft tissue samples. These tables include information about both the alpha and beta peaks, for either lead or arsenic. Tables 1 and 2 were both produced using data from the Canadian Light Source synchrotron, with table 1 showing the lead calibration slopes, and table 2 showing the arsenic calibration slopes. Tables 3 and 4 used the results from the InnovX portable XRF system, with table 3 showing the lead calibration slopes, and table 4 showing the arsenic calibration slopes. Table 5 and 6 show the calculated minimum detection limits from the lead and arsenic calibration lines, respectively.

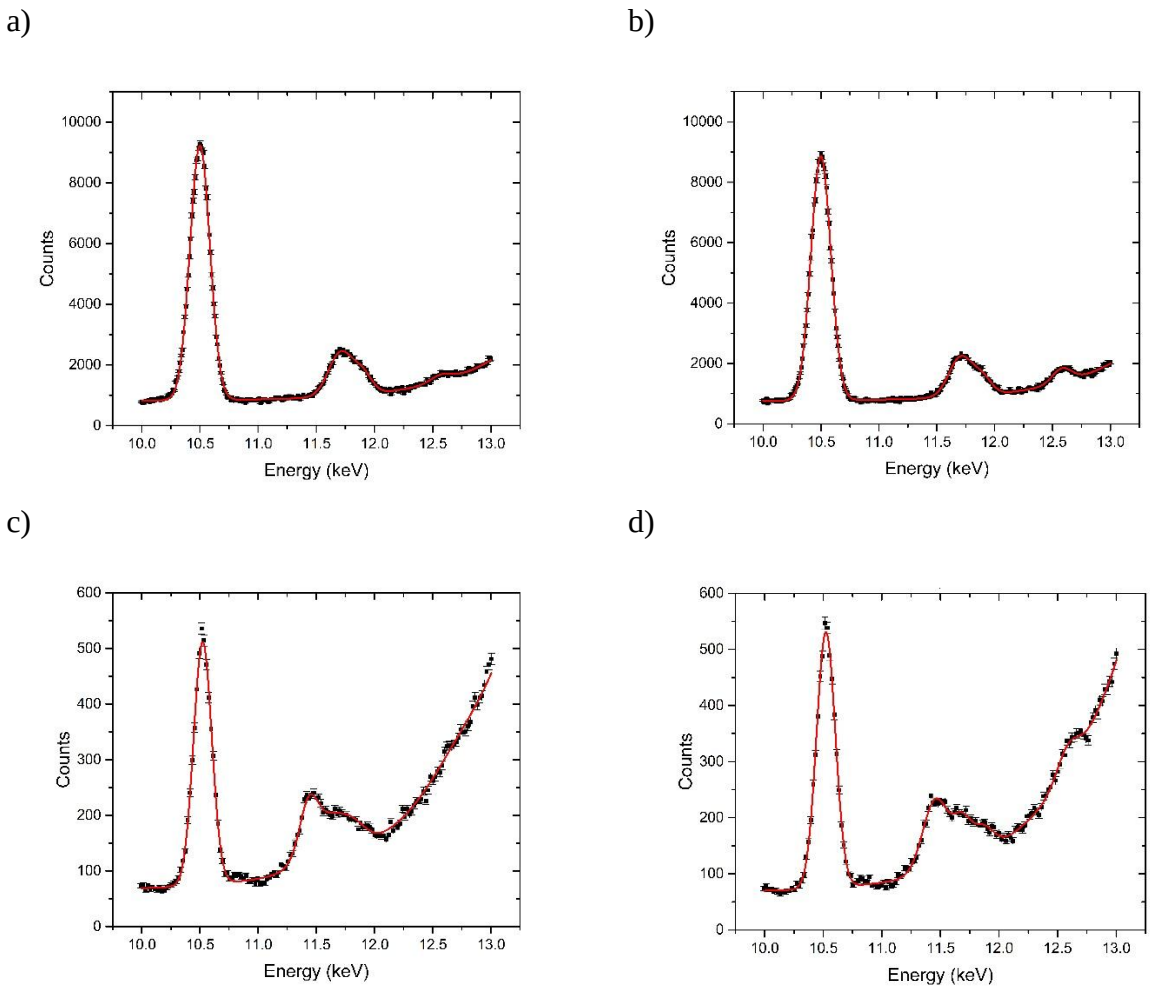

Figure 2. A comparison of XRF spectra of bone phantoms with 5 µg As g^{-1} in a thin soft tissue phantom from: a) the CLS synchrotron with 7 µg Pb g^{-1} in a bone phantom, b) the CLS synchrotron with 26 µg Pb g^{-1} in a bone phantom, c) the InnovX portable XRF system with 7 µg Pb g^{-1} in a bone phantom, and d) the InnovX portable XRF system with 26 µg Pb g^{-1} in a bone phantom.

Table 1. Synchrotron lead calibration line slopes, intercepts, and 0 ppm lead uncertainty with arsenic concentration kept constant.

	Pb Lα / As Kα Peak (10.5 keV)			*Pb Lβ Peak (12.6 keV)*		
Soft Tissue Phantom	*Slope [Counts/(μg Pb g^{-1})]*	*Intercept [Counts]*	*0 ppm Uncertainty [Counts]*	*Slope [Counts/(μg Pb g^{-1})]*	*Intercept [Counts]*	*0 ppm Uncertainty [Counts]*
Bare Phantom	73 ± 3	4 ± 36	10	73 ± 3	-28 ± 34	13
0 ppm As Thin	8.2 ± 0.4	36 ± 5	10	12 ± 2	28 ± 26	15
2 ppm As Thin	35 ± 20	2560 ± 200	20	24 ± 6	191 ± 64	15
5 ppm As Thin	42 ± 2	5843 ± 24	28	12 ± 1	56 ± 11	15
10 ppm As Thin	77 ± 21	11120 ± 310	49	10 ± 4	167 ± 53	19
0 ppm As Thick	5 ± 2	109 ± 34	11	5 ± 2	70 ± 36	18
2 ppm As Thick	12 ± 6	2393 ± 94	20	8 ± 1	211 ± 22	15
5 ppm As Thick	36± 25	7070 ± 370	38	7 ± 1	61 ± 18	20
10 ppm As Thick	47± 36	10880 ± 590	63	2.51 ± 0.03	100 ± 1	45

Table 2. Synchrotron arsenic calibration line slopes, intercepts, and 0 ppm arsenic uncertainty with lead concentration kept constant.

	As Kα / Pb Lα Peak (10.5 keV)			*As Kβ Peak (11.7 keV)*		
Lead ppm/Soft tissue thickness	*Slope [Counts/(μg As g^{-1})]*	*Intercept [Counts]*	*0 ppm Uncertainty [Counts]*	*Slope [Counts/(μg As g^{-1})]*	*Intercept [Counts]*	*0 ppm Uncertainty [Counts]*
0 ppm Pb Thin	1124 ± 32	100 ± 100	16	135 ± 27	159 ± 76	58
7 ppm Pb Thin	1201± 71	170 ± 150	9.1	183 ± 25	120 ± 48	33
17 ppm Pb Thin	1288 ± 42	218 ± 97	10	197 ± 10	94 ± 28	31
26 ppm Pb Thin	1243 ± 38	202 ± 88	11	184 ± 16	104 ± 27	32
0 ppm Pb Thick	1260 ± 130	80 ± 280	11	122 ± 1	77 ± 5	38
7 ppm Pb Thick	1170 ± 95	210 ± 250	12	129 ± 3	145 ± 2	36
17 ppm Pb Thick	1220 ± 150	270 ± 340	12	111 ± 3	116 ± 12	39
26 ppm Pb Thick	1320 ± 130	230 ± 310	12	145 ± 8	121 ± 7	45

Table 3. InnovX portable XRF lead calibration line slopes, intercepts, and 0 ppm lead uncertainty with arsenic concentration kept constant.

	Pb Lα / As Kα Peak (10.5 keV)			*Pb Lβ Peak (12.6 keV)*		
Soft Tissue Phantom	*Slope [Counts/(µg Pb g^{-1})]*	*Intercept [Counts]*	*0 ppm Uncertainty [Counts]*	*Slope [Counts/(µg Pb g^{-1})]*	*Intercept [Counts]*	*0 ppm Uncertainty [Counts]*
Bare Phantom	6.6 ± 0.1	1 ± 2	1.8	5.9 ± 0.6	20 ±10	14
0 ppm As Thin	0.6 ± 0.1	0 ± 3	2.2	1.1 ± 0.1	10 ± 2	9.3
2 ppm As Thin	0.8 ± 0.8	180 ± 20	4.9	1.7 ± 0.7	20 ± 20	15
5 ppm As Thin	1.11 ± 0.04	428 ± 1	7.2	1.8 ± 0.2	1 ± 5	18
10 ppm As Thin	1.2± 0.2	772 ± 5	7.4	1.8 ± 0.1	5 ± 2	4.3
0 ppm As Thick	0.3 ± 0.1	3 ± 2	2.4	0.5 ± 0.1	14 ± 2	10
2 ppm As Thick	1.0 ± 0.2	174 ± 3	4.3	1.7 ± 0.3	15 ± 5	5.8
5 ppm As Thick	1.0 ± 0.1	407 ± 2	11	0.9 ± 0.1	6 ± 3	16
10 ppm As Thick	1.0 ± 0.4	833 ± 8	10	0.9 ± 0.2	5 ± 4	8.1

Table 4. InnovX portable XRF arsenic calibration line slopes, intercepts, and 0 ppm arsenic uncertainty with lead concentration kept constant.

	As Kα / Pb Lα Peak (10.5 keV)			*As Kβ Peak (11.7 keV)*		
Lead ppm/Soft tissue thickness	*Slope [Counts/(µg As g^{-1})]*	*Intercept [Counts]*	*0 ppm Uncertainty [Counts]*	*Slope [Counts/(µg As g^{-1})]*	*Intercept [Counts]*	*0 ppm Uncertainty [Counts]*
0 ppm Pb Thin	78 ± 2	7 ± 8	2.7	1 ± 5	39 ± 9	25
7 ppm Pb Thin	80 ± 4	10 ± 10	2.7	10 ± 1	31 ± 3	54
17 ppm Pb Thin	80 ± 6	26 ± 20	2.8	8 ± 1	35 ± 2	42
26 ppm Pb Thin	81 ± 4	20 ± 10	2.8	5 ± 1	33 ± 3	40
0 ppm Pb Thick	82 ± 1	5 ± 3	2.4	6 ± 3	37 ± 5	32
7 ppm Pb Thick	84 ± 1	5 ± 3	2.4	5 ± 2	29 ± 5	59
17 ppm Pb Thick	84 ± 1	8 ± 2	2.4	7 ± 1	28 ± 1	51
26 ppm Pb Thick	84 ± 3	13 ± 8	2.3	8 ± 2	23 ± 3	42

Table 5. Lead calibration line minimum detection limits in units of μg Pb g^{-1}

	Synchrotron		*InnovX Portable XRF*	
Soft tissue phantom	Pb Lα / As Kα Peak MDL	Pb Lβ Peak MDL	Pb Lα / As Kα Peak MDL	Pb Lβ Peak MDL
Bare Bone	0.42 ± 0.02	0.52 ± 0.02	0.82 ± 0.01	7.3 ± 0.7
0 ppm As Thin	3.8 ± 0.2	3.7 ± 0.5	10 ± 2	26 ± 2
2 ppm As Thin	1.7 ± 0.9	1.9 ± 0.5	20 ± 20	30 ± 10
5 ppm As Thin	2.0 ± 0.1	3.5 ± 0.2	19 ± 1	30 ± 4
10 ppm As Thin	1.9 ± 0.5	6 ± 2	18 ± 4	6.9 ± 0.4
0 ppm As Thick	6 ± 2	10 ± 4	24 ± 8	70 ± 20
2 ppm As Thick	5 ± 2	6 ± 1	13 ± 2	10 ± 2
5 ppm As Thick	3 ± 2	9 ± 2	34 ± 3	53 ± 8
10 ppm As Thick	4 ± 3	53 ± 1	30 ± 10	28 ± 6

Table 6. Arsenic calibration line minimum detection limits in units of μg As g^{-1}

	Synchrotron		*InnovX Portable XRF*	
Lead ppm/Soft tissue thickness	As Kα / Pb Lα Peak MDL	As Kβ Peak MDL	As Kα / Pb Lα Peak MDL	As Kβ Peak MDL
0 ppm Pb Thin	0.042 ± 0.001	1.3 ± 0.3	0.102 ± 0.003	50 ± 170
7 ppm Pb Thin	0.023 ± 0.001	0.55 ± 0.07	0.100 ± 0.005	17 ± 2
17 ppm Pb Thin	0.0245 ± 0.0008	0.47 ± 0.02	0.105 ± 0.008	15 ± 2
26 ppm Pb Thin	0.0269 ± 0.0008	0.52 ± 0.04	0.104 ± 0.005	22 ± 5
0 ppm Pb Thick	0.026 ± 0.003	0.93 ± 0.01	0.088 ± 0.001	17 ± 8
7 ppm Pb Thick	0.030 ± 0.002	0.83 ± 0.02	0.086 ± 0.001	30 ± 20
17 ppm Pb Thick	0.029 ± 0.003	1.06 ± 0.03	0.0850 ± 0.0007	22 ± 2
26 ppm Pb Thick	0.028 ± 0.003	0.94 ± 0.05	0.083 ± 0.003	16 ± 3

a) b)

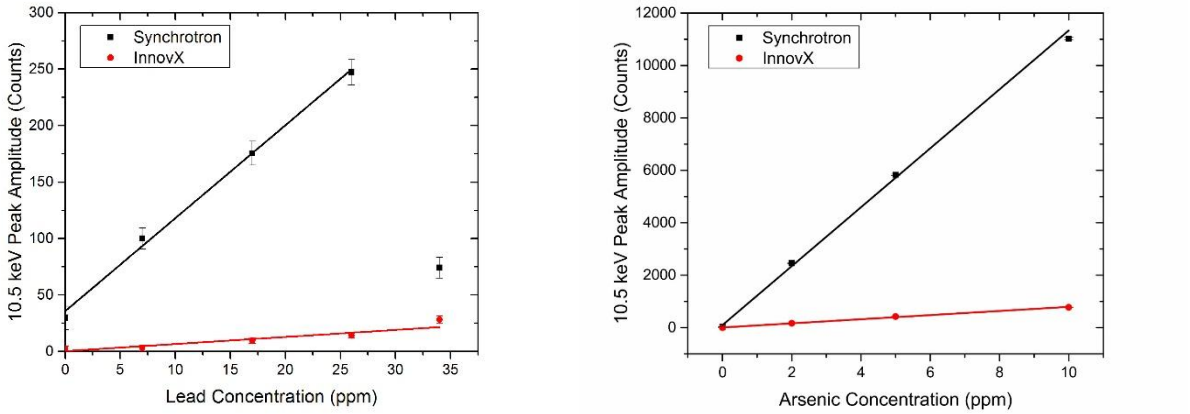

Figure 3. Examples of calibration lines produced by both the synchrotron and the portable InnovX XRF systems for the 10.5 keV peak. a) Shows the calibration line produced when lead concentration in the bone phantom is varied under a 0 ppm arsenic thin soft tissue phantom. (Note that the 34 ppm lead synchrotron data point is not included in the linear fit, as explained in the text.) b) Shows the calibration line produced when arsenic concentration is varied in a thin soft tissue phantom over a 0 ppm lead bone phantom.

Discussion

From the figure 2 comparison of spectra, it is notable that the peak amplitudes from the synchrotron (Figure 2 a) and b)) are significantly higher than their InnovX counterparts (Figure 2 c) and d)). There also appears to be less interference around the 11.7 keV As Kβ peak on the synchrotron compared to the InnovX. This is due to the presence of gold in the InnovX system, which makes it more difficult to successfully model the As Kβ peak amplitude. Both the synchrotron and InnovX system show a bromine Kα peak at 11.9 keV as bromine is found in the commercial resin. This is the reason the arsenic peak appears to have a more square shape for the synchrotron data, and this also contributes to interference in the InnovX spectra, further complicating the fitting of its As Kβ peak.

Figure 2 also shows an interesting comparison for when lead concentration is increased. Figure 2 a) and c) both contain 5 μg As g^{-1} in a thin (3.1 mm) soft tissue phantom and 7 μg Pb g^{-1} in bone, while figure 2 b) and d) contain 5 μg As g^{-1} in a thin soft tissue phantom and 26 μg Pb g^{-1} in bone. The most striking difference when lead concentration is increased is the clear emergence of the Pb Lβ peak at 12.6 keV. This peak is very difficult to see at lower concentrations, especially in 2 c), where it is almost entirely within the exponential background. Although a bit more challenging to see, it also appears that the combined As Kα and Pb Lα peak at 10.5 keV has a larger amplitude in b) and d), as would be expected with an increase in lead concentration. This slight increase implies that most of the amplitude in the combined peak comes from the presence of arsenic in the sample, as a much larger increase would be expected if lead dominated.

Figure 3 provides other important points of comparison. In both plots a) and b) of figure 3 the synchrotron produces a significantly steeper calibration slope than the InnovX system. A steeper calibration slope is associated with a lower minimum detection limit, suggesting the synchrotron would be optimal for detecting trace elements in humans. This result is due to the high photon fluence rate synchrotron x-ray beam, the well-tuned energy of excitation of the beam, and the use of the 4-element x-ray detector. When comparing figure 3 a) to figure 3 b), one can see that the arsenic calibration slope is steeper than that of lead for both the synchrotron and the portable XRF system. This shows again that arsenic is the more efficient contributor to the 10.5 keV peak when both lead and arsenic are present in a sample. Problems could arise if one was attempting to measure bone lead in a person who has high concentrations of arsenic in their overlying tissue. In this case, one could use the lead Lβ peak at 12.6 keV to measure lead content, or check for the presence of the arsenic Kβ peak at 11.7 keV.

Tables 1 through 4 demonstrate that the intercept of the combined lead Lα and arsenic Kα calibration line increases as the constant concentration of arsenic or lead is increased. This increase is linear, and results directly from the increasing background arsenic or lead values. Comparing tables 1 to 3, and tables 2 to 4, the slopes, intercepts, and uncertainties were all much higher in data taken at the CLS synchrotron. Again, this is due to the higher count rates resulting from the synchrotron. Higher slopes are also associated with the lower minimum detection limits presented in tables 5 and 6. When comparing the slopes created from lead calibration lines (tables 1 and 3) to those from arsenic (tables 2 and 4), the trend of higher arsenic calibration slopes mentioned previously is seen across all tested combinations. Tables 1 through 4 also contain all data relevant to the calculation of the minimum detection limits seen in tables 5 and 6.

The results shown in tables 1 through 4 display a considerable amount of variation, even in cases where they would be expected to be similar from one condition to the next. For example, in table 1 pertaining to the synchrotron measurements, the slope of the lead Lβ peak relation under the condition of a 0 ppm arsenic thin phantom is clearly different than the slope of the lead Lβ peak relation under the condition of a 2 ppm arsenic thin phantom. These variations propagate through to also contribute to differences in minimum detection limits in tables 5 and 6. We attribute these variations to a combination of effects. It is possible that small-scale inhomogeneities in concentration or physical density exist in both the lead- and arsenic-dosed phantoms. Depending on the point of irradiation, this could result in unusually high or low results from a given reading. Likewise, any slight variation in thickness in the arsenic-dosed soft tissue phantoms would introduce an additional source of variation due to either differences in excitation volume (for the arsenic signal) or differences in attenuation (for the lead signal). Combined with statistical uncertainties, such effects can be substantial. It is recommended that future synchrotron work

carefully consider the homogeneity of the phantoms through repeat measurements at variation locations.

When examining the minimum detection limits seen in tables 5 and 6, the synchrotron clearly outperforms the portable XRF system. To some extent, this is simply a consequence of a greater number of incident photons. However, this advantage of the synchrotron is further enhanced by other factors. Using data collected from the samples using 0 ppm of lead in bone phantoms, and 2 ppm, 5 ppm, and 10 ppm of arsenic in thin soft tissue phantoms, it was found that the average number of photons counted across the entire energy spectrum at the synchrotron was 4.2 times higher than the number of photons from the portable system. However, the 10.5 keV arsenic Kα peak amplitude was 14 times higher for the synchrotron. This demonstrates that the monochromatic nature of the synchrotron beam (more efficient excitation of characteristic x-rays) makes an important contribution to the difference in signal between the two approaches. Other benefits of the synchrotron derive from the size and polarization of its beam, reducing the background noise relative to the portable system.

An even more obvious difference between the two approaches can be seen when comparing the systems' abilities to detect beta peaks. The portable InnovX system must compete with interference from gold when fitting for the arsenic Kβ peak, and a large exponential background curve that interferes with the lead Lβ peak (see figure 2 c) and d)). This exponential background is caused by the broad range of x-ray energies produced by the portable system. Many of these x-rays scatter and enter the detector creating the background interference. The synchrotron does not have the same issue of gold interference and, more importantly, has a reduced spectral background due to a reduced number of Compton scatter events occurring at various angles – a direct consequence of the small size of the incident x-ray beam. Therefore, the synchrotron is

better at detecting small amplitude peaks. This is important if attempting simultaneous detection of lead and arsenic, as the combined peak at 10.5 keV may not provide sufficient information. A past study of bone lead in workers from high lead environments found some lead levels to be over 100 μg Pb g^{-1} in the human tibia [Fleming *et al*. 1997]. Both the synchrotron and the InnovX system had minimum detection limits well below this value, under all scenarios. Another trend which emerges is each system's ability to detect trace amounts of arsenic more readily than trace amounts of lead. The excitation of arsenic by the incident x-ray beam and the escape and subsequent detection of arsenic K shell x-rays are enhanced by the location of this element in the superficial soft tissue phantom. In contrast, bone lead excitation and L-shell x-ray intensities are diminished by x-ray attenuation caused by the overlying soft tissue. Using the same definition of minimum detection limit, a past study completed with arsenic in soft tissue phantoms found a minimum detection limit of 0.67 μg As g^{-1} using a portable XRF system [Fleming and Gherase 2007]. From the table 6 results with the new InnovX portable XRF system, it is clear that capabilities have improved in the last decade. These improvements may be largely traced to higher beam currents and the use of a silicon drift detector.

Table 5 demonstrates the effect overlying soft tissue has on lead detection in bone. Without any overlying soft tissue phantom, both the InnovX system and the synchrotron produce the lowest minimum detection limits. When a thin (3.1mm thick) soft tissue phantom is added, the minimum detection limits increase. They increase even more when a thick (3.9 mm) soft tissue phantom is used. (The only exception to this was with the 2 μg As g^{-1} thin soft tissue result from the InnovX system. This result, however, had a very large uncertainty.) The overall trend is consistent with expectation. A recent feasibility study using portable XRF found minimum detection limits for lead under soft tissue of 3 mm thickness (similar to the thin soft tissue

phantoms used here) to be 4.6 ppm, and under soft tissue of 4 mm thickness (similar to the thick soft tissue phantoms used here) to be 8.0 ppm, using three-minute measurements [Specht *et al*. 2014]. The results presented above from the synchrotron are superior to those values, while results from the InnovX portable XRF system are slightly worse.

Conclusion

Although the synchrotron data in this study indicate significantly better sensitivity relative to the portable XRF method, the synchrotron approach is by no means ideal. Synchrotrons are mostly research-dedicated facilities with only a small fraction of time available for recurring procedures such as a potential medical application. They are also expensive to build and operate, and do not meet the basic accessibility requirements of medical practice or public health. Furthermore, dosimetry considerations would be prohibitive. Using the photon fluence rate determined from the VESPERS beamline, we calculated a dose rate of ~0.3 Gy/s, for a dose of ~36 Gy from a 120 second measurement. This compares with a maximum measured dose rate of 4×10^{-4} Gy/s from a portable system [Gherase *et al.* 2010] which, if corrected for the beam current used in this study, suggests a maximum dose rate of $\sim 2 \times 10^{-3}$ Gy/s, and a maximum dose of ~1.2 Gy (from five 120 second repeat measurements). Clearly, dose reductions would be required before either approach could be considered for *in vivo* application, and as expected the synchrotron dose is exceedingly large. On the other hand, synchrotron radiation is monochromatic, polarized and highly collimated – all highly desirable properties for research involving XRF trace element detection. Varying synchrotron parameters such as the incident energy, or the angle between the beam and detector, could help in the development and optimization of a portable XRF system designed *specifically* for trace element detection in humans. Feasibility studies have demonstrated potential for portable XRF bone lead measurement in humans [Nie *et al*. 2011;

Fleming *et al.* 2011; Specht *et al*. 2014], and early *in vivo* assessments have recently been completed [Specht et al. 2016]. In the long term, improvements to such systems could allow for large studies of remote populations on the effects of exposure to various trace elements. Future work specific to the lead in bone and arsenic in soft tissue interference could focus on improving the separation of the arsenic Kα signal from the lead Lα signal. The Kβ/Kα and Lβ/Lα ratios are fundamental atomic constants, previously measured and calculated, and can be taken from the literature [Garg *et al*. 1984; Scofield 1974]. Provided that proper x-ray attenuation corrections are made, the ratios can be used to determine the magnitude of one of the overlapping peaks. For example, if the lead Lβ was measured, the amplitude of the corresponding lead Lα peak may be calculated from the known value of the lead Lβ/Lα ratio. These topics will form the focus of future work involving both synchrotron radiation and a dedicated portable XRF approach.

Acknowledgements

This work was supported by a Discovery Grant from the Natural Sciences and Engineering Research Council of Canada. Student travel to the Canadian Light Source was made possible by a President's Research and Creative Activity Award from Mount Allison University. We gratefully acknowledge the assistance of Renfei Feng and Peter Blanchard at the VESPERS beamline. Research described in this paper was performed at the Canadian Light Source, which is supported by the Canada Foundation for Innovation, Natural Sciences and Engineering Research Council of Canada, the University of Saskatchewan, the Government of Saskatchewan, Western Economic Diversification Canada, the National Research Council Canada, and the Canadian Institutes of Health Research.

References

Abernathy C O, Thomas D J and Calderon R L 2003 Health effects and risk assessment of arsenic J. Nutr. 133 1536S-1538S

Desouza E D, Abu Atiya I, Al-Ebraheem A, Wainman B C, Fleming D E B, McNeill F E and Farquharson M J 2013 Characterization of the depth distribution of Ca, Fe and Zn in skin samples, using synchrotron micro-x-ray fluorescence (SμXRF) to help quantify in-vivo measurements of elements in the skin Appl. Radiat. Isot. 77 68-75

Fleming D E B, Boulay D, Richard N S, Robin J-P, Gordon C L, Webber C E and Chettle D R 1997 Accumulated body burden and endogenous release of lead in employees of a lead smelter Environ. Health Perspect. 105 224-233

Fleming D E B, Gherase M R and Alexander K M 2011 A miniature x-ray tube approach to measuring lead in bone using L-XRF X-ray Spectrom. 40 343-347

Fleming D E B, Gherase M R and Anthonisen M 2013 Calibrations for measurement of manganese and zinc in nail clippings using portable XRF X-ray Spectrom. 42 299-302

Fleming D E B and Gherase M R 2007 A rapid, high sensitivity technique for measuring arsenic in skin phantoms using a portable x-ray tube and detector Phys. Med. Biol. 52 N459-N465

Garg M L, Singh J, Verma H R, Singh N, Mangal P C and Trehan P N 1984 Relative intensity measurements of L-shell x-rays for Ta, Au, Pb and Bi in the energy range 17-60 keV J. Phys. B: At. Mol. Phys. 17 577-584

Gherase M R and Fleming D E B 2011 A calibration method for proposed XRF measurements of arsenic and selenium in nail clippings Phys. Med. Biol. 56 N215-N225

Gherase M R, Mader J E and Fleming D E B 2010 The radiation dose from a proposed measurement of arsenic and selenium in human skin Phys. Med. Biol. 55 5499-5514

Goyer R A 1993 Lead toxicity: current concerns Environ. Health Perspect. 100 177-187

Grolimund D, Senn M, Trottmann M, Janousch M, Bonhoure I, Scheidegger A M and Marcus M 2004 Shedding new light on historical metal samples using micro-focused synchrotron x-ray fluorescence and spectroscopy Spectrochimica Acta Part B 59 1627-1634

Nie L H, Sanchez S, Newton K, Grodzins L, Cleveland R O and Weisskopf M G 2011 *In vivo* quantification of lead in bone with a portable x-ray fluorescence system – methodology and feasibility Phys. Med. Biol. 56 N39-N51

Rabinowitz M B 1991 Toxicokinetics of bone lead Environ. Health Perspect. 91 33-37

Schwartz R A 1997 Arsenic and the skin Intl. J. Derma. 36 241-250

Scofield J H 1974 Exchange corrections of K x-ray emission rates Phys. Rev. A 9 1041-1049

Somervaille L J, Chettle D R and Scott M C 1985 *In vivo* measurement of lead in bone using x-ray fluorescence Phys. Med. Biol. 30 929-943

Specht A J, Lin Y, Weisskopf M, Yan C, Hu H, Xu J and Nie L H 2016 XRF-measured bone lead (Pb) as a biomarker for Pb exposure and toxicity among children diagnosed with Pb poisoning Biomarkers 21 347-352

Specht A J, Weisskopf M and Nie L H 2014 Portable XRF technology to quantify Pb in bone *in vivo* Journal of Biomarkers Article ID 398032, 9 pages

Todd A C 2002 L-shell x-ray fluorescence measurements of lead in bone: theoretical considerations Phys. Med. Biol. 47 491-505

Todd A C, Carroll S, Geraghty C, Khan F A, Moshier E L, Tang S and Parsons P J 2002 L-shell x-ray fluorescence measurements of lead in bone: accuracy and precision Phys. Med. Biol. 47 1399-1419

Williams G P (2001) Electron binding energies In X-Ray Data Booklet, Second Edition, pp. 1-1 – 1-7 Lawrence Berkeley National Laboratory, Berkeley, CA